Shahrood University of Technology
Iranian Society of Mining Engineering (IRSME)
Journal of Mining and Environment (JME)
journal homepage: www.jme.shahroodut.ac.ir
THOMSON REUTERS
Vol. 10, No. 1, 2019, 223-240.
DOI: 10.22044/jme.2019.7535.1607

A comparison between effects of earthquake and blasting on stability of mine slopes: a case study of Chadormalu open-pit mine

R. Shafiei Ganjeh[1*], H. Memarian[1], M.H. Khosravi[1] and M. Mojarab[2]

1. School of Mining Engineering, College of Engineering, University of Tehran, Tehran, Iran
2. Bonyan Zamin Paydar Consultant Engineers, Tehran, Iran

Received 12 October 2018; received in revised form 15 January 2019; accepted 16 January 2019

Keywords

Chadormalu Mine
Seismic Hazard Analysis
Numerical Modelling
Dynamic Slope Stability
Earthquake
Blasting

Abstract

Dynamic slope stability in open-pit mines still remains a challenging task in the computational mining design. Earthquake and blasting are two significant sources of dynamic loads that can cause many damages to open-pit mines in active seismic areas and during exploitation cycles. In this work, the effects of earthquake and blasting on the stability of the NW slope of Chadormalu mine are compared by a numerical modeling method. The dynamic results show that the maximum displacement under earthquake and blasting loads within the slope are 844 mm and 146 mm, respectively. According to the shear strain results, both the earthquake and blasting waveforms are destructive, while the earthquake waveforms cause more damages to the slope. Moreover, the deterministic and probabilistic seismic hazard analyses are carried out to assess the seismicity of the mine area. The experimental results indicate that the maximum values for the vertical and horizontal accelerations are 0.55 g and 0.75 g, respectively. The maximum calculated acceleration is then scaled to the selected earthquake accelerograms. In order to show the effective impact of the established scale, the model is executed using the original accelerograms. The results obtained show that the established scale prevents overestimation and underestimation of the displacement and strain. Therefore, applying scaled accelerograms in a dynamic slope stability analysis in mine slopes leads to more reliable and robust results. The overall results show that a strong earthquake causes plenty of damages to the slope, and consequently, interrupts the mining cycle. Hence, the seismic study and dynamic slope stability should be considered as a part of the computational mining design.

1. Introduction

The dynamic slope stability analysis is a significant scope in geotechnical engineering, and is generally assessed by implying numerical modeling methods. Applying these techniques will lead to obtain stress distribution and deformation state. However, the use of physical modeling in the simulation of geotechnical and mining problems has acquired a worldwide acceptance, especially by the development of geotechnical centrifuge machines [1]. Though, due to the complexity of the failure mechanism, numerical modeling is still more reliable for simulation of heterogeneous and anisotropic materials as rock masses [2]. Rock slopes such as open-pit mine slopes suffer from induced damages that are caused by dynamic loads including earthquake and blasting. For example, on July 1990, a 5.3 magnitude earthquake triggered a rotational landslide at the Panluo open-pit mine in SW Fujian Province in China [3]. On the other hand, Hoek (1975) has proposed that although blasting waves are not capable of inducing major instabilities in mine slopes, stability of individual benches of the pit is affected by near surface damages caused by these waves [4]. Such instabilities in pit benches can expose main roads

Corresponding author: roshanakshafiei@ut.ac.ir (R. Shafiei Ganjeh).

of the mine, and consequently, delay the exploitation cycle. Therefore, studying the effects of dynamic loads in open-pit mines plays an important role in the computational mining design and exploitation.

The stability of open-pit slopes has been considered in various research works. For instance, Read and Stacey published a guideline for designing open-pit slopes [5]. Moreover, an index called MSII has been introduced to assess the instability of open-pit mine slopes [6]. In most recent research works, the critical parameters such as rainfall, blasting method, and geometry of the slope are used to analyze the stability of open-pit slopes by means of artificial neural networks [7] and the quantitative hazard assessment system [8].

In the past decades, several researchers have been engaged in dynamic slope stability using the numerical modeling methods. Based on our best knowledge, as the first attempt, Clough (1960) introduced an engineering analysis called the finite element method (FEM) on the basis of the mathematical approach first developed by Courant (1943) [9, 10]. The stability of slopes under earthquake load has been widely considered in the literature. Seed et al. (1973) and Wilson and Keefer (1983) conducted dynamic slope stability analyses on earthquake-induced landslides [11, 12]. In addition, non-linear inelastic soil models in two-dimensions and three-dimensions have been developed and implemented in the earthquake-induced dam and landslide models [13-15]. Some relevant topics have also been considered in this scope such as the seismic stability analysis of rock slope by means of the finite difference method (FDM) [16], comparison between different slope stability analysis methods during an earthquake [17], involving the influence of the tension failure on the seismic slope stability by FDM [18] dynamic slope stability analysis using real accelerograms as seismic load [19], and developing a safety factor calculation model in dynamic phase based on the Hoek-Brown failure criterion [20]. In more recent works, the effects of earthquake on open-pit mines in seismically active areas have been considered [21]. The dynamic slope stability analysis has also been carried out where the dynamic load has been performed based on the expected peak ground acceleration of the studied area [22]. Moreover, the stability analysis of the earthquake-induced rock slopes and the relativity of their failure mode to the actual condition of the material parameters have been analyzed [23]. Xiong and Huang (2017) have considered the parameters that affect the dynamic stability of slopes, mentioning the variability and uncertainties in components [24]. Fan et al. (2018) have presented a new seismic input method that considers near-field oblique incidence based on the mechanisms of artificial viscous boundaries and the influence of incident angle on the dynamic response of rock slopes. Accordingly, the most damaging incident direction has been recognized as perpendicular to the slope surface [25]. In another study, the stability of the NE slope of the Daralou open-pit mine against a secondary toppling failure has been studied by means of FEM to predict the behavior of the final slope in static and dynamic conditions [26]. In addition, the shaking table tests have recently been noted in the dynamic slope stability field [27, 28]. Lin et al. (2018) developed a method to investigate the behavior of a dip slope under the shaking table test, while Song et al. (2018) clarified the dynamic stability of a rock slope by means of the shaking table tests and discussed the effects of discontinuities and rapid drawn down on the slope during the earthquakes. However, despite the earthquake load, the effect of blasting waves on the stability of slopes has been dealt with in limited studies. The stability of rock slopes subjected to the blasting load has been analyzed using the discrete element method (DEM) [29, 30] and FEM [31]. In most recent research works, Jiang et al. (2017) studied the influence of underground mining blasting on the stability of open-pit slopes using FEM [32], and Zheng et al. (2018) proposed an effective and simple model to preliminary assess the stability of rock slopes based on the degree of blasting damage [33]. Generally, the seismic slope stability has been investigated considering different numerical approaches including FEM [19, 26, 31, 32], FDM [16, 18, 34], and DEM [29, 30].

In this work, we studied and compared the effects of earthquake and blasting on the stability of mine slopes. Here, the stability of the NW slope of the Chadormalu mine was analyzed under both the earthquake and blasting loads using a numerical modeling method. Besides, the seismicity of the Chadormalu mine was estimated based on the deterministic (DSHA) and probabilistic seismic hazard analyses (PSHA). In addition, for modeling the earthquake and blasting loads, the actual waveforms from three destructive events and three recorded explosions at the mine site were applied. To determine the stability of the slope, a numerical model was established base on FDM. The model was then analyzed using both

the static and dynamic approaches to obtain the stability condition in either states.

The rest of this paper is organized as what follows. In Section 2, the geological features of the case slope are presented. In Section 3, the proposed methods for this work including seismic hazard analysis, dynamic load preparation, and numerical modeling are stated. Results and discussion are presented in Section 4, and conclusions are drawn in Section 5.

2. Geological features of case slope

The Chadormalu mine is one of the largest iron reserves in Iran. It is located in an active seismic area that experienced destructive earthquakes such as Tabas (1978, Mw: 7.7) and Zarand (2005, Mw: 6.5). In addition, blasting operation in the Chadormalu mine is inevitable in the exploitation cycle. The geographical location of the Chadormalu mine, the geological map and the section of the slope under study (AA'), and the approximated trace of the AA' section on the pit are shown in Figures 1, 2 and 3, respectively.

Despite the high strength of formative rocks, the slope has suffered from instabilities due to several faults establishing fracture zones. As shown in Figure 4, nine faults are recognized within the slope. Rock weathering in surface layers of the slope is also another reason for the observed instabilities. The F-a fault shown in Figure 4 exhibits a strike-slip fault perpendicular to the slope surface. Back in 2012, as the exploitation procedure had moved forward, some movements were observed in the F-a fault hanging wall toward the center of the pit. Monitoring the results showed that the movements were compatible with the occurrence of a 4.8 magnitude earthquake on March 15, 2012. Tension cracks were also observed around the installed monitoring pins (Figure 5).

Geotechnical investigations and site-monitoring observations showed that the tension cracks appearing on top of the slope were growing and leading to instabilities in different levels of the slope. Some of these tension cracks and minor instabilities of the slope are shown in Figure 6.

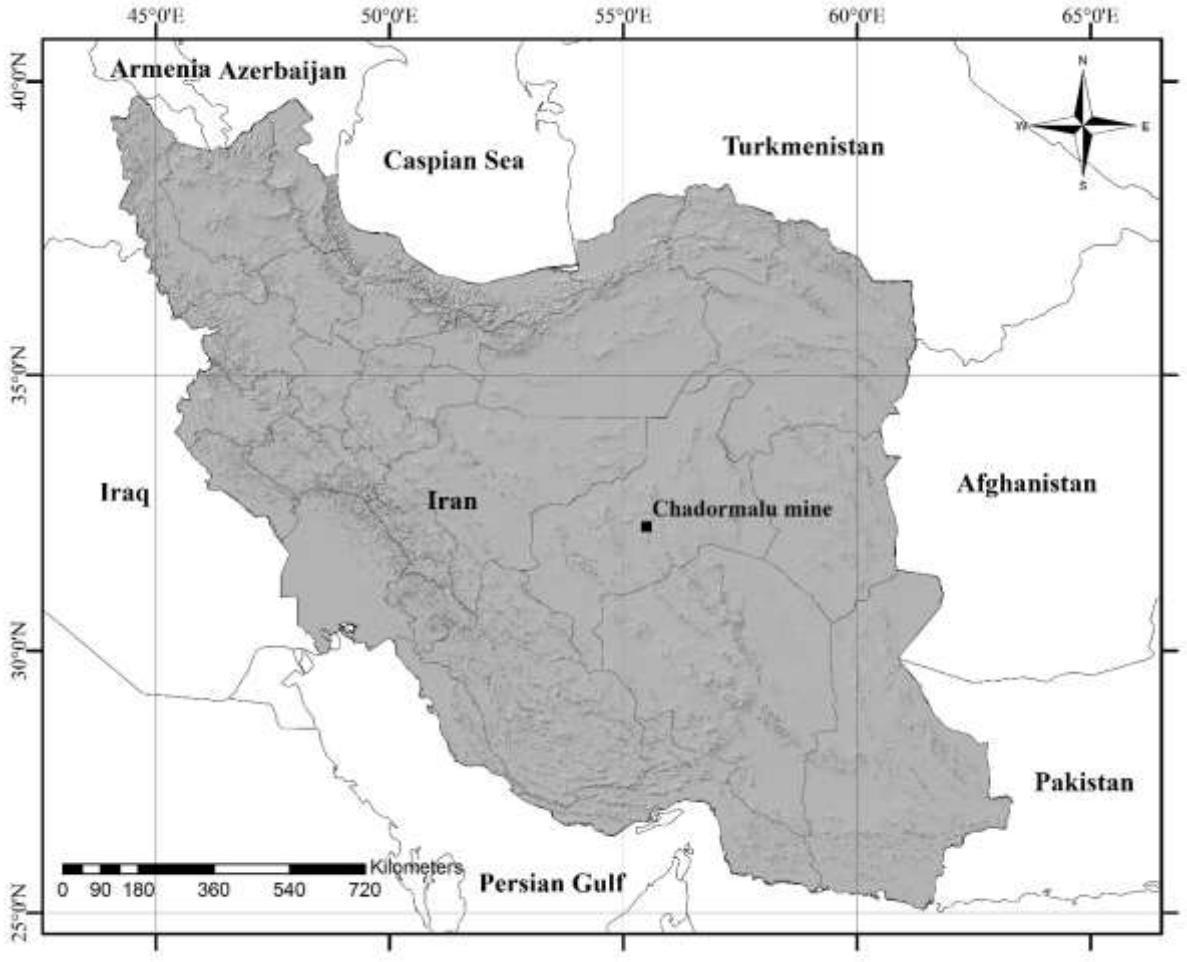

Figure 1. Geographical location of Chadormalu iron ore mine in Yazd Province in Iran.

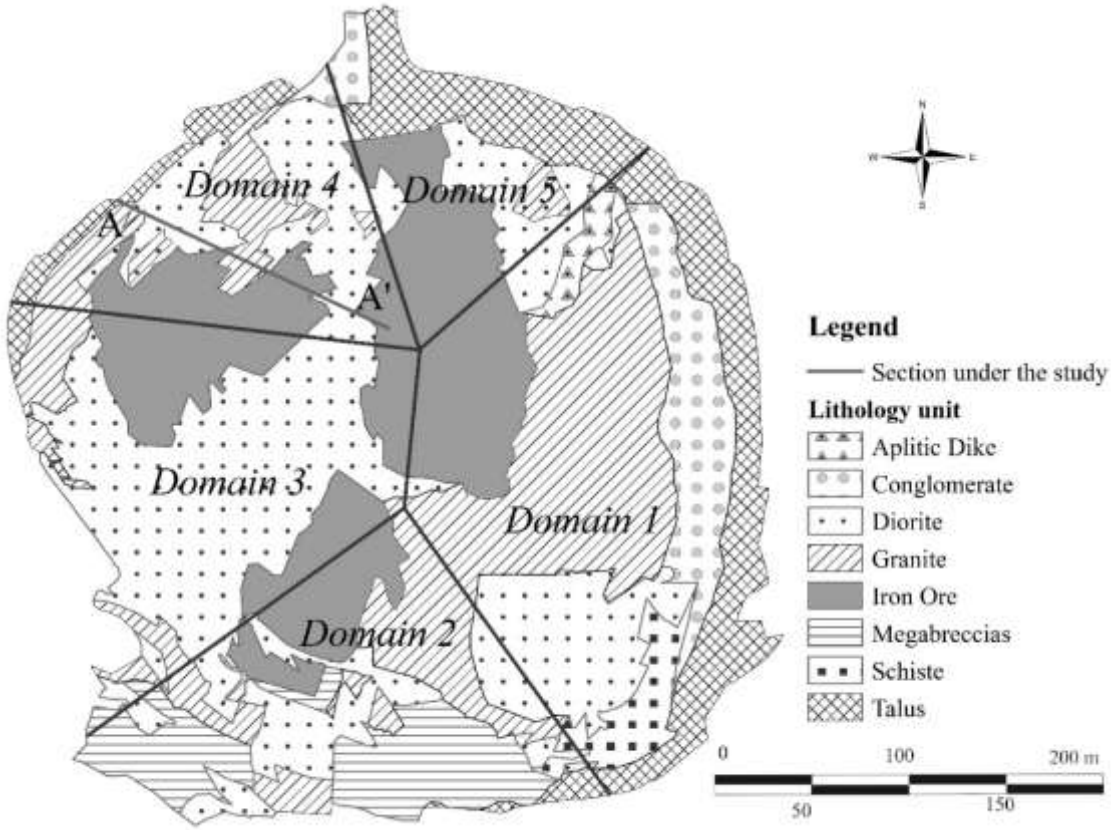

Figure 2. Geological map of Chadormalu mine showing five domains of the pit and the section under study (AA') in domain 4.

Figure 3. The approximated trace of the section under study (AA') on the NW slope of Chadormalu mine.

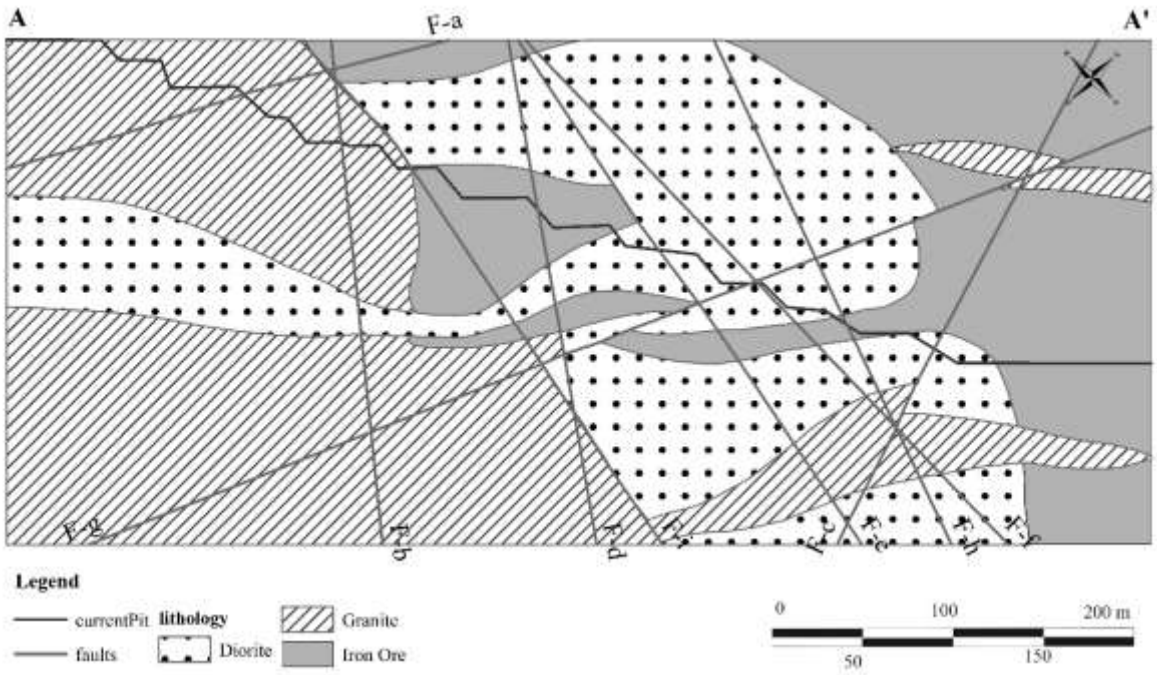

Figure 4. The section under study (AA') exhibiting current pit, faults including F-a fault, and rock types.

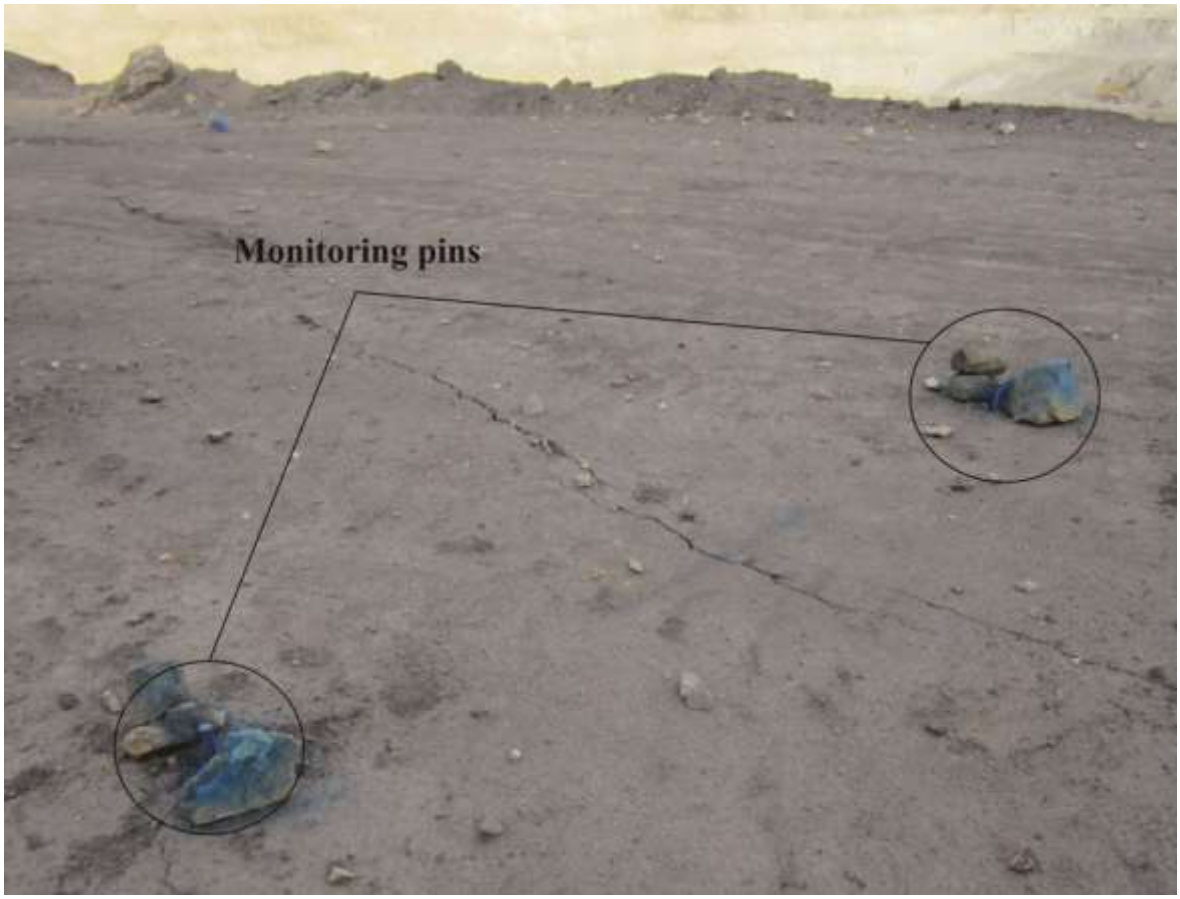

Figure 5. The installed monitoring pins to monitor the displacements around the F-a fault hanging wall on top of the slope under study. Tension cracks are observed around these pins.

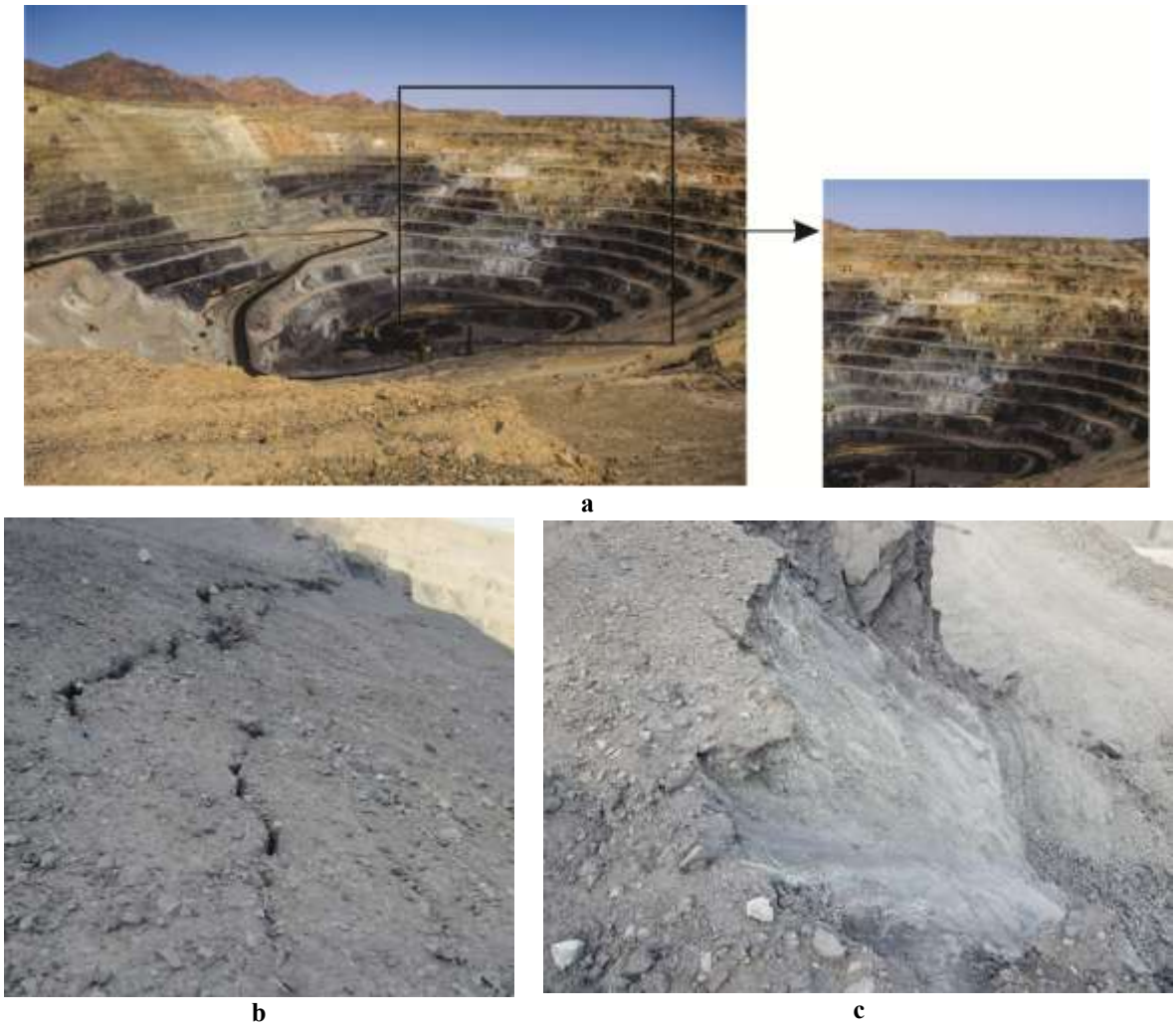

Figure 6. Tension cracks and minor instabilities of the slop. a: Location of the tension cracks on top of the slope (shown in black rectangle); b: Tension cracks on top of the slope; c: Minor instability (planar failure) observed within the slope.

3. Materials and methods

In the proposed method, initially, the seismic hazard analysis was carried out by the DHSA and PSHA approaches. Afterwards, the dynamic loads including collected earthquakes and recorded blasting waves were prepared to perform the slope stability analysis. In the next sub-sections, the details of the seismic hazard analysis, dynamic load preparation, and numerical modeling process are stated.

3.1. Seismic hazard analysis

The purpose of the seismic hazard analysis is to determine a ground motion with its associated occurrence interval and the uncertainties at a site of interest [35]. The DHSA and PSHA methods play a significant role in the seismic hazard analysis and complement each other to provide additional insights for seismic problems [36]. In the DHSA approach, the parameter of interest was assessed for an earthquake with a specific magnitude and a constant source-to-site distance [37]. On the other hand, in the PSHA method, the effects of different magnitudes, recurrence time, epicentral location, and amplitude of the interested parameter were taken under consideration [38, 39].

In this work, all the recorded earthquakes since 1911 in 150 km radial distance of the Chadormalu mine with a moment magnitude (Mw) greater than 4 were collected for the seismic hazard analysis (Figure 7). Based on the DSHA approach, each recorded earthquake was assigned to a seismic source. The peak ground acceleration (PGA) in both the horizontal and vertical directions was calculated by Zare (1999) using the attenuation relationship developed for Iran [40]. The maximum calculated vertical and horizontal PGA values using the DSHA approach were 0.55 g and 0.75 g, respectively. In order to estimate the probability based on the PSHA approach, three distinct probabilities including distance,

magnitude, and PGA were calculated. Finally, the calculated probabilities of all seismic sources were combined. The hazard curve for the Chadormalu mine based on the PSHA approach with a 475-year return period is shown in Figure 8.

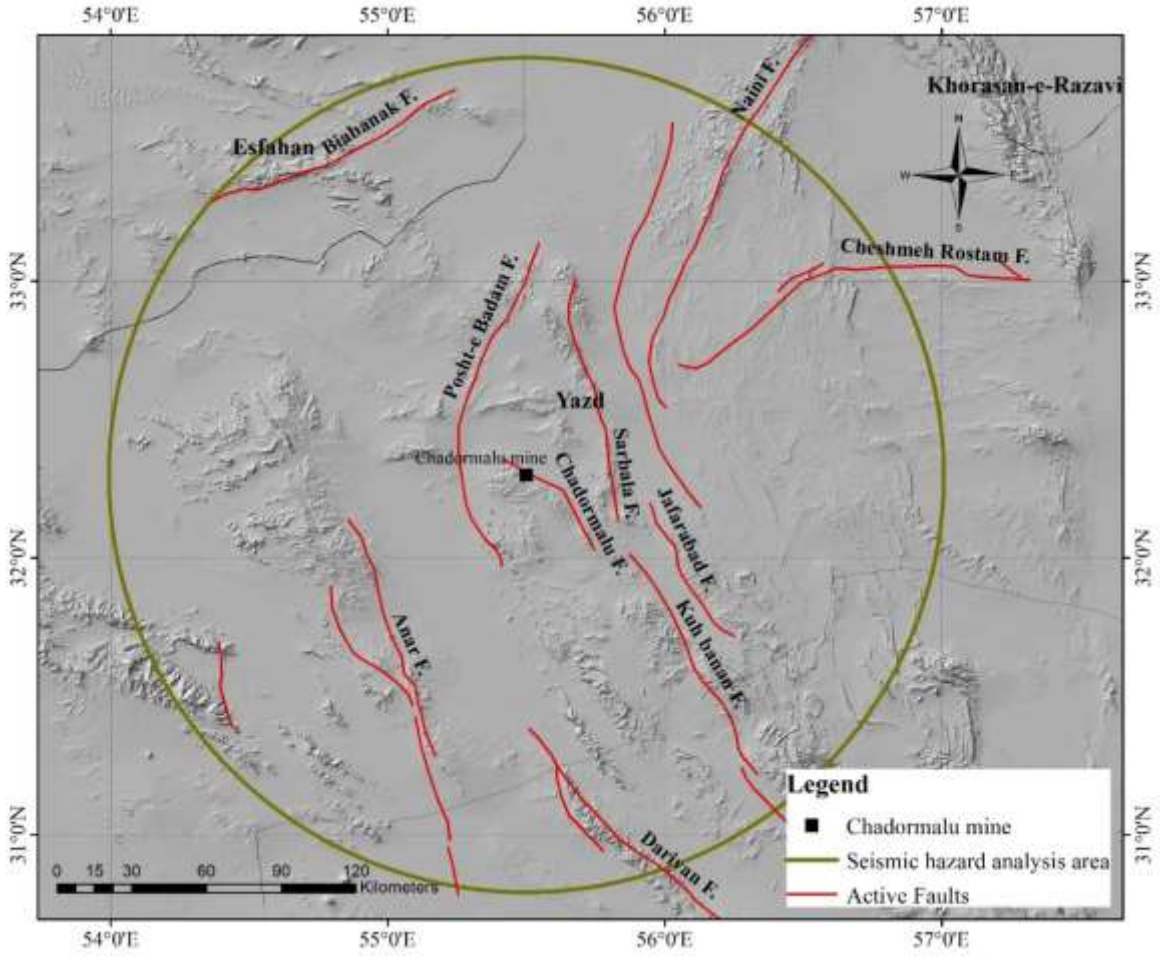

Figure 7. Seismic hazard analysis area and active faults in 150 km radial distance of Chadormalu mine.

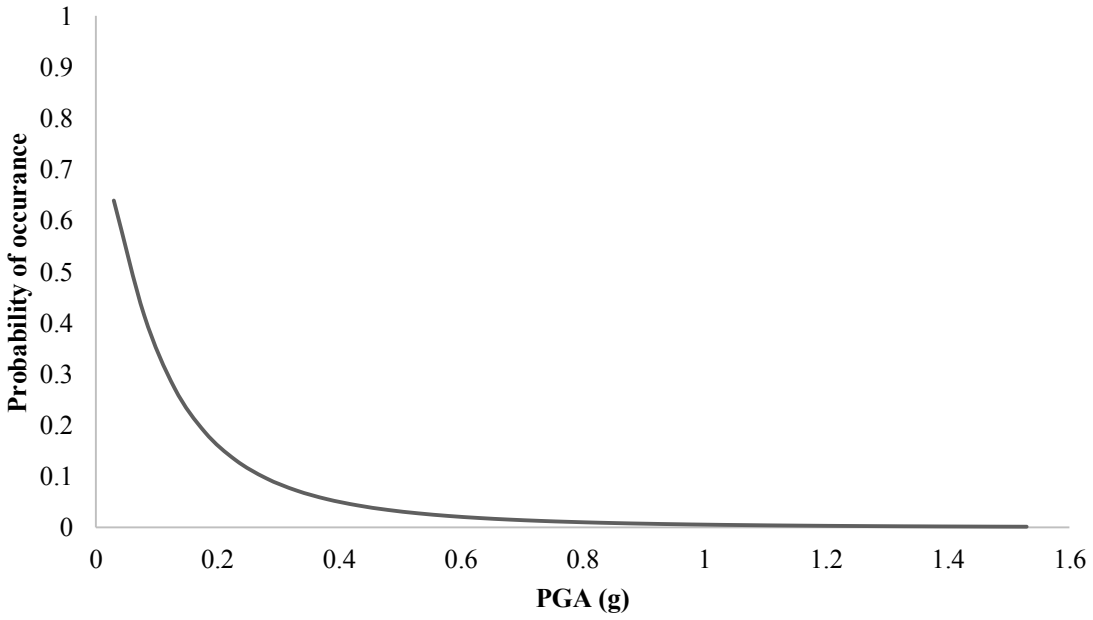

Figure 8. The hazard curve of Chadormalu mine based on PSHA approach with a 475-year return period.

3.2. Dynamic load preparation

In the earthquake dataset, the transverse component of the acceleration history of the Tabas, Zarand, and Zanjiran earthquakes has been adopted as sources of dynamic loads rather than the commonly used sinusoidal wave. The Tabas and Zarand events happened in the central-Iran zone, which is the same seismotectonic zone as the Chadormalu mine, while the Zanjiran earthquake occurred in another seismotectonic zone, i.e. Zagros [41].

The Tabas earthquake occurred in September 16, 1978. The surface magnitude (Ms) of this event was declared to be 7.4. The depth of this earthquake was estimated to be 34 km. The selected accelerogram belonged to the Deyhook station at the 33.29 North latitude and 57.5 East longitude geographical coordination [42]. The Tabas event is a near fault earthquake that can properly simulate the effect of the Chadormalu fault seismic activity on the site.

The Zanjiran earthquake happened in June 20, 1994 in the Fars district in Iran. The depth of this 5.7 Ms event was declared to be 8 km. The selected accelerogram was taken from the Zanjiran station at the 29.88 North latitude and 52.62 East longitude geographic coordination. The highest recorded acceleration in the Alpine-Himalayan orogenic belt, i.e. 1.006 g belongs to the Zanjiran event [43]. As shown in Figure 10(b), the waveform of this event begins with a high acceleration impact, the same as the blasting waves. Therefore, the results of this event are comparable to the blasting results and also confirm the effects of the seismotectonic zone on the waveforms.

The Zarand earthquake took place in February 22, 2005. The Mw value for this event was declared to be 6.5. The earthquake happened at a 10 km depth. The selected accelerogram was chosen from the Bafgh station at the 31.63 North latitude and 55.42 East longitude geographic coordination [44]. The rupture of the Kuhbanan fault was recognized as the cause of this event. The Kuhbanan fault is one of the seismic sources within our seismic hazard study, and this makes the Zarand earthquake a significant event in the dataset. The location of all the three mentioned accelerograms are shown in Figure 9.

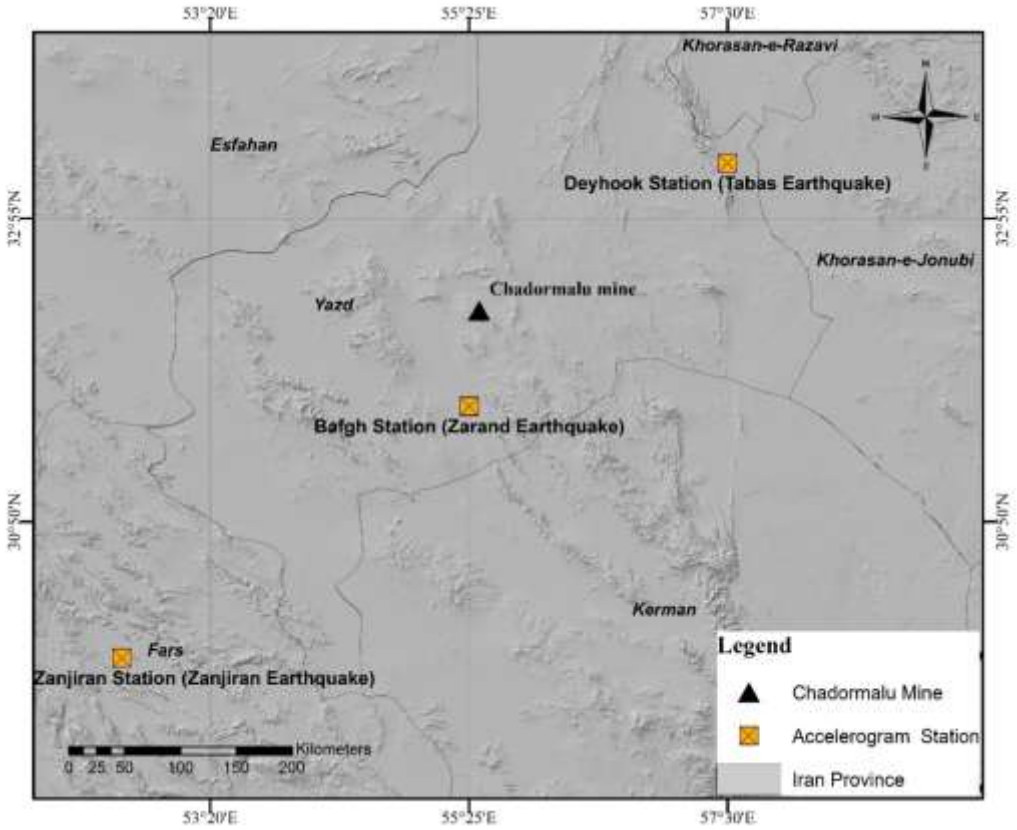

Figure 9. Location of Deyhook, Bafgh, and Zanjiran stations that recorded Tabas, Zarand, and Zanjiran events, respectively.

In order to adjust the selected accelerograms to the site condition, the maximum calculated acceleration obtained for the DSHA approach was scaled to the mentioned earthquake accelerograms. Therefore, the peak acceleration of each accelerogram used was equal to 0.75 g. The waveforms of the scaled earthquakes are shown in Figure 10.

In the blasting dataset, three blasting operations were recorded using the Guralp CMG-6TD seismometer at the Chadormalu mine. The blasting waves were recorded in three blocks at different distances from the seismometer (Figure 11). Moreover, the characteristics of the blocks are summarized in Table 1. Based on Figure 11, the B1 and B3 blocks have experienced the most and the least accelerations, and are also located in the closest and farthest distance from the blasting source, respectively.

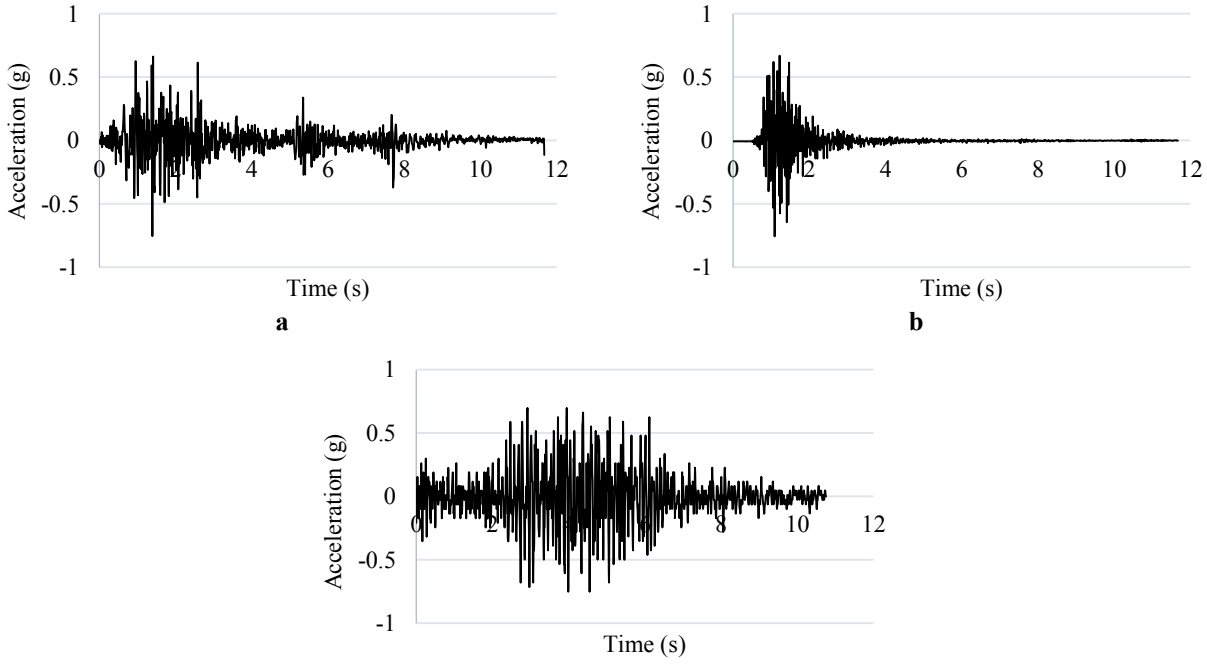

Figure 10. The waveforms of the scaled earthquakes. a: Tabas; b: Zanjiran; and c: Zarand events.

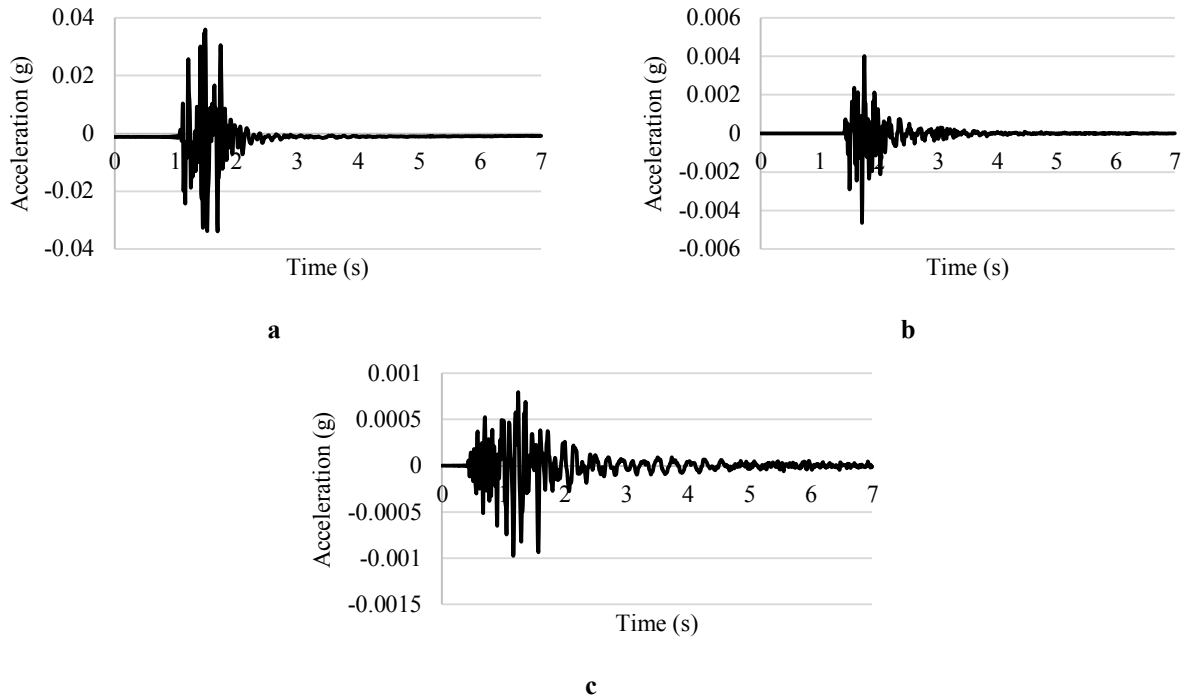

Figure 11. The recorded blasting waves assigned to (a): block B1, (b): block B2, and (c): block B3.

Table 1. Characteristics of the recorded blasting waves in different blocks.

Block number	Lithology	Explosive weight (kg)	Level (m)	Distance from seismometer (m)
B1	Waste	214.40	1570	158.6
B2	Ore-Waste	150.50	1590	415.1
B3	Waste	725.50	1390	1566.8

In order to estimate the transferred energy of blasting to the blocks, an experimental relationship was used [45]:

$$E_T = \eta_1 \eta_2 Q E_e \quad (1)$$

where E_T is the transferred energy from one hole to the rock, Q is explosive weight in each hole, E_e is the explosive specific energy, and η_1 and η_2 are the impedance and coupling coefficients provided according to Equations 2 and 3, respectively [45]:

$$\eta_1 = 1 - \frac{(I_r - I_e)^2}{(I_r + I_e)^2} \quad (2)$$

$$\eta_2 = \frac{1}{e^{\varphi_h/\varphi_c} - (e-1)} \quad (3)$$

where I_r is the rock impedance, I_e is the explosive impedance, φ_h is the hole diameter, and φ_c is the explosive diameter. The measured transferred energy of the recorded blasting waves to the blocks are summarized in Table 2. According to this table, the B3 block, due to its explosive weight, experiences the highest energy level.

Table 2. The measured impedance, coupling coefficients, and transferred energy of blasting waves.

Block number	Impedance coefficients	Coupling coefficients	Transferred energy from each hole to rock (MJ)
B1	0.81	0.54	346.90
B2	0.81	0.54	243.60
B3	0.81	0.19	413.10

3.3. Numerical modeling

The numerical modeling methods are common in solving the dynamic slope stability problems [46]. While employing these methods, there is no need to make assumptions about the shape or location of the failure surface, forces, and their directions [47]. The most commonly utilized methods in numerical rock mechanical models are continuum (FDM, FEM, and boundary element (BEM)), Discrete (DEM, and discrete fracture network (DFN)), and Hybrid methods. The choice of continuum or discrete methods mainly depends on the problem scale and fracture system geometry. The continuum approach is suitable in situations where only few fractures are present, and fracture opening and complete block detachment are not significant factors [48]. According to the highly fractured nature of the slope under study, the continuum methods seem applicable [16, 49].

Among the continuum methods, BEM is more suitable for solving problems with fracturing inhomogeneous and linearly elastic bodies [48], which make it inapplicable in our case. In this work, FDM was chosen over FEM. The basic of FDM is based upon the direct discretization of governing partial differential equations (PDEs) carried out by replacing the partial derivatives with differences defined at neighboring grid points. On the other hand, the FEM development was specifically oriented towards rock mechanics problems. This is because it was the first numerical method with enough flexibility for the treatment of material heterogeneity, non-linear deformability (mainly plasticity), complex boundary conditions, *in situ* stresses, and gravity [48]. However, according to the significant progress in the ability to generate irregular meshes such as quadrilateral grids and the application of this method in the time domain with properly chosen time stepsΔt, FDM was employed in this work. Because of the time domain solution, the function values at time t can be inferred from values at t_Δt. Moreover, unlike FEM and BEM, no local trial or interpolation functions were applied to estimate PDE in the sampling point neighborhoods. Hence, FDM is the most direct and intuitive technique in the PDE solution [50].

The section under study composes of Granite, Diorite, and Ore in wide speared regions as well as nine faults. To involve the faults in our model, 10 m zones around each fault were considered as the fault zones. Because of the frequently fractured nature of the slope, Mohr-Coulomb constitutive model was selected for the analysis. The rock mechanical properties of the slope are summarized in Table 3 [51].

Table 3. Rock mechanical properties of the slope material [51].

Rock type parameter	Granite	Diorite	Ore	Faulted zone
Bulk density (kg/m^3)	2400	2800	3700	2300
Bulk modulus (MPa)	1466.67	1000	7333.3	466.67
Shear modulus (MPa)	880	600	4400	280
Cohesion (MPa)	0.23	0.23	0.9	0.07
Friction angle	37^o	34^o	50^o	17^o
Tension strength (MPa)	0.02	0.03	0.14	0.0005

The model was generated based on the size of the slope, i.e. 600 m long and 270 m height. Afterwards, the desired model was meshed for an accurate wave transmission using Equation 4 [52]:

$$\Delta l \le \frac{C_s}{10f} \tag{4}$$

where Δl is the element length, C_s is the shear wave velocity, and f is the dominant frequency of the seismic input load. The element length was calculated using the parameters presented in Table 4. In the earthquake dataset, dominant frequencies as strong motion parameters were taken from the earthquake accelerograms. In the blasting dataset, dominant frequencies of the records were calculated based on the horizontal to vertical spectral ratio (HVSR) method [53]. Moreover, the shear wave velocity is a site-dependent parameter that is measured in each station. As shown in Table 4, the minimum value obtained for the element length was 1.36 m. Accordingly, the size of the model elements was considered 1 m in both the horizontal and vertical directions to fulfil the Kuhlmeyer and Lysmer law for all the earthquake and blasting records and avoid distortion in the model.

In order to reach the static balance and properly reconstruct the site condition, the model was excavated in six steps, where two benches were cut in each step. The procedure was repeated until all benches were excavated (Figure 12). Then the model base was fixed in the horizontal and vertical directions, while both sides of the model were fixed only in the horizontal direction. With regard to the executed model, the best calculated factor of safety (FoS) was 1.59. Besides, the potential failure surface was observed to be between 1315 and 1330 m levels, where the strike of the F-e, F-g, and F-f faults intersected with the surface of the slope (Figure 13). In order to develop the desired dynamic model, some modifications are required to be conducted through the balanced static model. Application of fixed defined boundary conditions of the static model in the dynamic mode causes the seismic wave reflects inside the model, and consequently, the necessary energy radiation will not happen. To figure out this challenge, the free field boundary developed by Lysmer and Kuhlmeyer (1969) [54] was applied on both sides of the model, yet the base was fixed in both the horizontal and vertical directions.

To figure out the effects of non-uniform grids, the calculation of critical time step involves both mass and stiffness at each degree of freedom. Based on Equation 5, the value of 7.5×10^{-5} was calculated as the critical time step required for stability of the slope during the dynamic execution.

$$\Delta_{tcrit} = \frac{A_z}{L_d C_p} \tag{5}$$

In Equation 5, C_p is the longitudinal wave velocity, A_z is the area of the zone, and L_d is the length of its diagonal. In the time-domain analysis, damping is simulated by the Rayleigh formulation based on Equation 6 [55]. In this formula, a damping matrix is used with components proportional to mass (M) and stiffness (K):

$$C = \alpha M + \beta K \tag{6}$$

where C is the damping matrix, and α and β are the mass-proportional and stiffness-proportional damping constants, respectively. For a geological material, damping falls between 2% to 5% [56]. Due to the plastic flow and low shear strength, a considerable loss of dynamic energy might occur in the dynamic analysis. Therefore, in such models where significant displacements are expected, a minimal percentage of damping is required. In the current work, the proper Rayleigh damping percentage was estimated based on the comparison between the resulting acceleration history and the earthquake waveforms. The selected damping ratio for all earthquakes are listed in Table 5.

Table 4. The applied parameters in the model element length calculation.

Waveform	Shear wave velocity (m/s)	Dominant frequency (HZ)	Element length (m)
Tabas earthquake	780	25	3.12
Zarand earthquake	462	10	4.62
Zanjiran earthquake	680	50	1.36
Blasting records (average value)	714.6	13.8	5.4

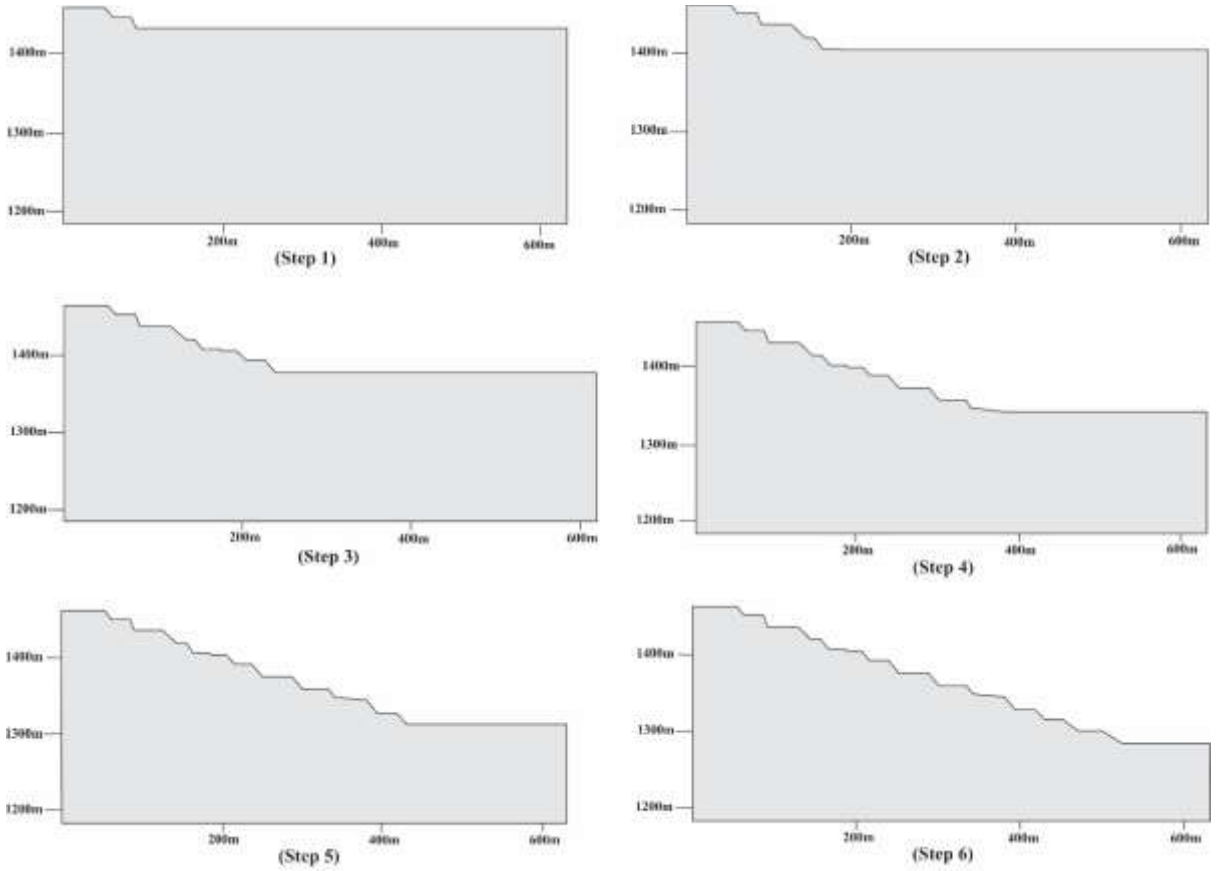

Figure 12. Process of excavating the numerical model in six steps before static execution. Two benches are cut in each step.

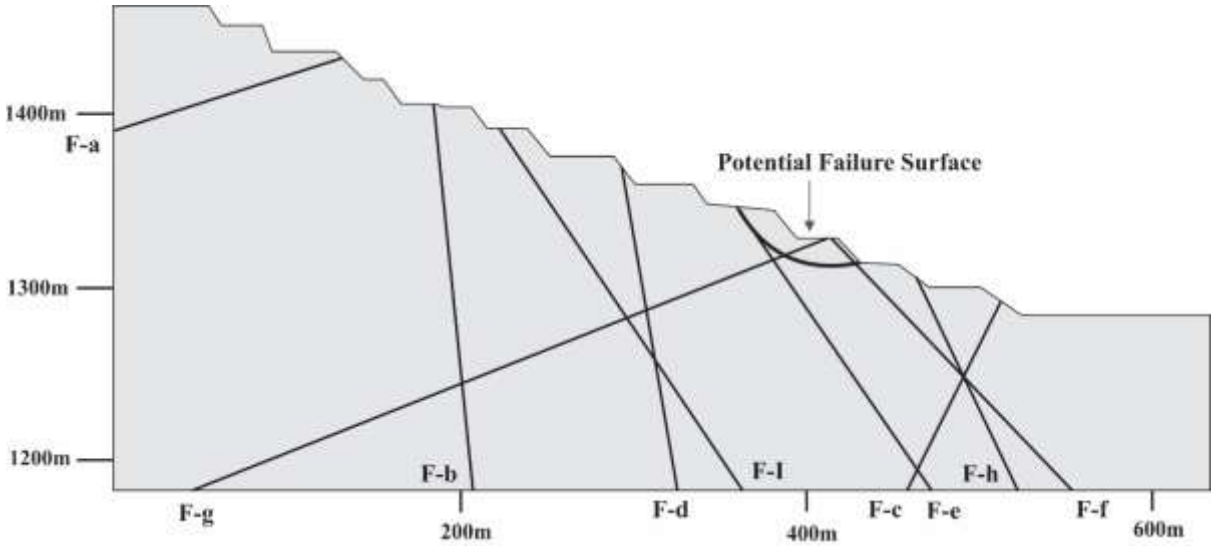

Figure 13. Potential failure surface of the section under study (AA') due to static execution. The potential failure surface is located in intersection of F-e, F-g, and F-f faults strike with surface of slope between 1315 and 1330 m levels.

Table 5. Critical damping ratio of the earthquakes.

Earthquake	Critical damping ratio (%)
Tabas	5
Zarand	0.7
Zanjiran	0.7

To control the sharp waves such as blasting, the artificial damping was used. This damping consists of the Von Neumann (q_1) and Landshoff (q_2) parameters, as Equation 7 [57, 58].

$$q = a_n q_1 + a_L q_2 \quad (7)$$

In Equation 7, a_n and a_L are constant parameters, which, in this case, are supposed to be 1. Besides, q_1 and q_2 are defined as Equations 8 and 9, respectively:

$$q_1 = bc_0^2 \rho L^2 \dot{\varepsilon}^2 \quad (8)$$

$$q_2 = bc_1 \rho L_a \dot{\varepsilon} \quad (9)$$

where L is the characteristic zone dimension, $\dot{\varepsilon}$ is the zone volumetric rate, ρ is the zone density, a is the material p-wave speed equal to $\sqrt{\frac{(K + \frac{4}{3}G}{\rho}}$ (K and G are bulk and shear modulus of the zone), b is $-\mathrm{sgn}(\dot{\varepsilon})$, and c_0 and c_1 are the constants set to 1 and 2, respectively.

To input the earthquake motion at the free field boundary, the velocity waves of the earthquake records were converted to stress history using Equation 10.

$$\sigma_s = 2(\rho C_s v_s) \quad (10)$$

where σ_s is the applied shear stress, ρ is the mass density, C_s is the shear wave velocity propagation through medium, and v_s is the shear particle velocity. To input the inner forces such as blasting motion at the free field boundary, the measured velocity histories were used. Dynamic load as a time history is propagated through the model by spring and damper interaction. Hence, the displacement, velocity, and acceleration of each element were calculated based on the motion equations.

In order to determine the stability condition of the slope under dynamic loads, the critical shear strain criterion was applied. Sakurai et al. (1998) defined the critical shear strain as the ratio between the shear strength and the shear modulus, as Equation 11 [59].

$$\gamma_0 = \frac{\tau_c}{G} \quad (11)$$

The value for the critical shear strain for each layer of the slope was estimated and summarized in Table 6. In the analyses, if the calculated value passes the limit, the slope will be considered unstable.

Three mentioned earthquake accelerograms with the same peak acceleration (0.75 g) but different waveforms, and three blasting records were assigned to the model as the dynamic loads. The stress histories of the earthquakes were applied to the base of the model; however, the velocity histories of blasting records, based on the level of blasting operation, were applied to the side and upper part of the model. In the next section, the experimental results of the dynamic modeling are presented.

Table 6. The values for critical shear strain in different layers of the slope.

Rock type	Granite	Diorite	Ore	Faulted zone
Shear modulus (MPa)	880	600	4400	280
Shear strength (MPa)	28.13	23.18	60.50	5.27
Critical shear strain (%)	3.2	3.8	1.38	1.88

4. Results and discussion

The dynamic loads including the Tabas, Zarand, and Zanjiran earthquakes were applied to the model as 11.68, 10.76, and 12.80 s, respectively. The 7 s of the blasting records including their peak acceleration were also selected as the dynamic loads. The maximum displacement due to the earthquakes was observed in the results for the Zanjiran event and was about 844 mm (Figure 14). The slope experienced less displacement due to the Tabas earthquake but a wider range of damages between 1285 and 1330 m levels were formed in comparison with the Zanjiran event (Figure 15). In the unstable zone caused by the Tabas earthquake, the f-e, F-g, F-f, and F-h faults intersected with the surface of the slope. On the other hand, the created unstable zone by the Zanjiran earthquake was between 1285 and 1315

m levels, where the F-h and F-c faults intersected with the surface of the slope. The Zarand earthquake did not form any unstable zone within the slope.

The maximum displacement due to the blasting operation was observed due to the B2 block explosion, which was about 146 mm. All the three blasting waveforms caused an unstable zone between 1285 and 1315 m levels, which was the same as the Zanjiran earthquake (Figure 15). This is because of the occurrence of the mentioned earthquake in the Zagros seismotectonic zone, which is different from the Tabas and Zarand earthquake seismotectonic zones. Although the B3 block had the longest distance from the blasting source, the same unstable zone as B1 and B2 blocks was caused due to this explosion. This is because of the higher transferred energy from each hole to the B3 block. The results obtained from the dynamic loads on the stability of the slope under the study are summarized in Table 7.

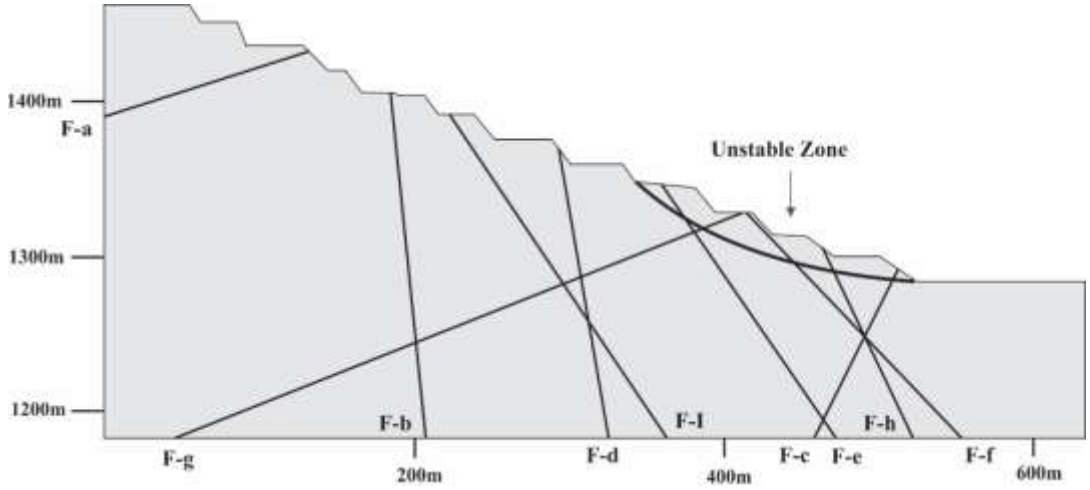

Figure 14. The unstable zone in the section under study (AA') due to Tabas earthquake.

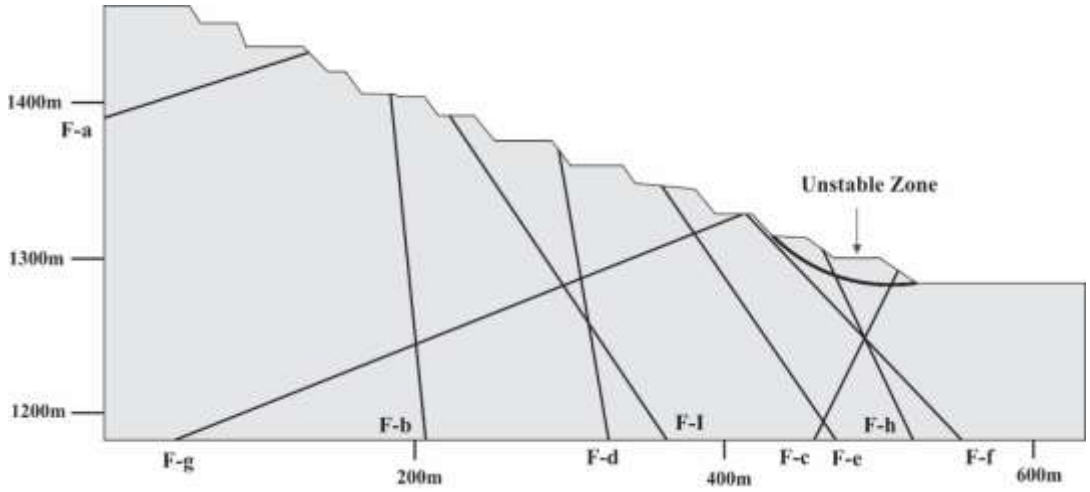

Figure 15. The unstable zone in the section under study (AA') due to Zanjiran earthquake and blasting waves.

Table 7. The results obtained for dynamic slope stability in the section under study.

Dynamic load	Event duration (s)	Maximum displacement (mm)	Maximum shear strain (%)	Stability condition
Tabas earthquake	11.68	450	17.5	Unstable
Zanjiran earthquake	12.8	844	30	Unstable
Zarand earthquake	10.67	80.8	3	Stable
B1-blast	6.5	125	7	Unstable
B2-blast	6.5	146	5	Unstable
B3-blast	6.5	140	10	Unstable

The results of the dynamic numerical model due to the earthquake loads were validated by the limit equilibrium method. The model was executed based on the quasi-static method considering 0.75 g horizontal acceleration. According to the Bishop approach, the factor of safety was 0.65 [60]. The potential failure surface was observed to be between 1285 and 1380 m levels (Figure 16). As shown in Figure 16, despite the same PGA, a wider unstable zone was obtained using the quasi-static method compared to FDM (Figure 16). This is because in the quasi-static method, acceleration is considered as a permanent load; however, in FDM, a waveform is applied to the model. Consequently, an extended unstable zone in the quasi-static method is acceptable. The results of the dynamic model due to the blasting records were validated according to the observed responses at the site.

As mentioned in Section 3.2, real accelerograms were adopted as the sources of the inputted dynamic loads and then scaled to the site's maximum calculated acceleration obtained for DSHA. In order to investigate the effective impact of the established scale, the model was executed using the Tabas and Zarand original accelerograms. The results of the scaled and original accelerograms are compared in Table 8. It can be observed that the scale procedure in a destructive event such as the Tabas earthquake prevents the overestimation of the results. As shown in Table 8, inputting the Tabas real accelerogram as dynamic load caused enhancement in both the maximum displacement and shear strain within the slope. On the other hand, the scale procedure in the Zarand earthquake prevents the underestimation of the results. As shown in this table, applying the Zarand real accelerogram as dynamic load reduced the maximum displacement and shear strain within the slope. Therefore, applying the scaled accelerograms in the dynamic slope stability analyses in mine slopes leads to more reliable and robust results.

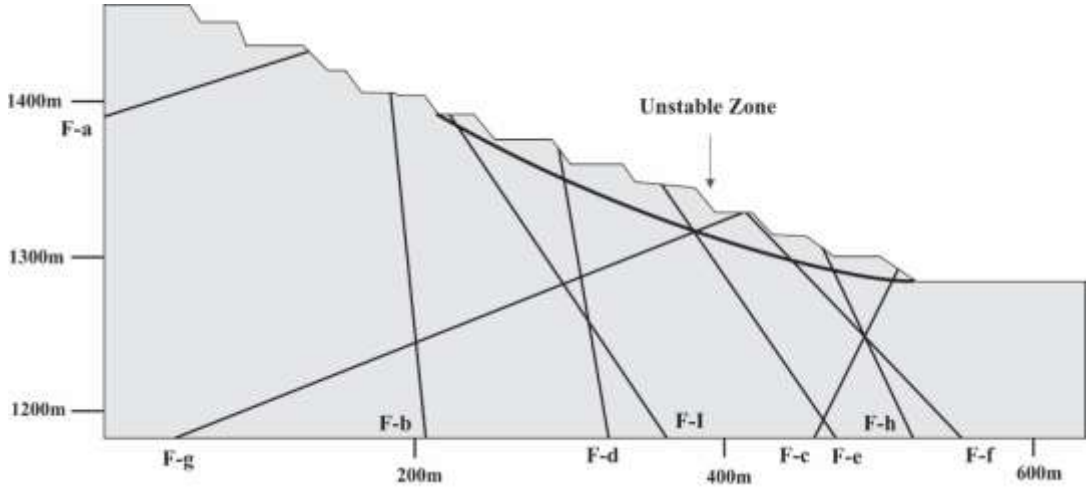

Figure 16. The unstable zone in the section under study (AA') due to quasi-static execution while applying 0.75 g horizontal acceleration.

Table 8. Comparison between the results of scaled and original accelerograms of Tabas and Zarand earthquakes in the dynamic slope stability analysis.

Event	Maximum displacement (mm)	Maximum shear strain (%)
Tabas scaled accelerogram	450	17.5
Tabas real accelerogram	1280	35
Zarand scaled accelerogram	80.8	3
Zarand real accelerogram	66	1.75

5. Conclusions

The aim of this work was to compare the effects of the earthquake and blasting loads on the stability of mine slopes. This objective was obtained by analyzing the stability of the Chadormalu NW slope under earthquake and blasting loads. The novelty of our work is in two folds. The first one is that we compared the earthquake and blasting effects on the stability of the mine slopes. The second one is using scaled earthquake waveforms following the seismic hazard analysis as dynamic loads. Accordingly, the following results were obtained:

- Based on DSHA, the maximum vertical and horizontal accelerations in the Chadormalu mine were 0.55 g and 0.75 g, respectively.
- According to PSHA, the probability of occurrence of a 0.75 g earthquake in the Chadormalu mine for a 475-year return period was 0.012.
- The static slope stability analysis showed that the slope was stable considering the calculated factor of safety as 1.59.
- Following the dynamic numerical modeling, based on the critical shear strain criterion, the slope was unstable under the Tabas and Zanjiran earthquakes. However, the Zarand earthquake did not cause an unstable zone in the slope. On the other hand, all the three blasting records caused instabilities within the slope.
- The unstable zone, caused due to the blasting records, and the Zanjiran earthquake are similar. This is because of the similarity of their waveforms, as the Zanjiran earthquake happened in the Zagros seismotectonic zone and exhibited a different waveform than the Tabas and Zarand earthquakes.
- The maximum displacements obtained under earthquake and blasting loads were 844 mm and 146 mm, respectively. Therefore, the overall damages caused by the earthquakes are more considerable than the blasting record damages.
- The established scale prevents the overestimation and underestimation of the displacement and strain, respectively, due to the Tabas and Zarand earthquake loads. Therefore, applying scaled accelerograms in dynamic slope stability analyses in mine slopes leads to more reliable and robust results.
- A strong earthquake can cause plenty of damages to the mine slopes, and consequently, interrupt the mining cycle. Hence, the seismic study should be considered as a part of a computational mining design.

Acknowledgments
The work presented here is part of a master thesis project. The authors would like to thank the Chadormalu mine management for data accommodation and cooperation in recording blasting waves as well as preparing field investigation at the mine site. The authors would also like to especially thank Mr. Hossein Izadi for his valuable comments.

References
[1]. Khosravi, M.H., Takemura, J., Pipatpongsa, T. and Amini, M. (2016). In-Flight Excavation of Slopes with Potential Failure Planes. Journal of Geotechnical and Geoenvironmental Engineering. 142 (5): 06016001.

[2]. Leelasukseree, C., Pipatpongsa, T., Khosravi, M.H. and Mavong, N. (2012). Stresses and a failure mode from physical and numerical models of undercut slope lying on inclined bedding plane. 7th Asian Rock Mechanics Symposium. Seoul. Korea. pp. 15-19.

[3]. Wei, Z., Yin, G., Wan, L. and Shen, L. (2008). Case history of controlling a landslide at Panluo open-pit mine in China. Environmental Geology. 54: 699-709.

[4]. Hoek, E. (1975). Influence of drilling and blasting on stability of slopes in open pit mines and quarries. Proc, Atlas Copco Bench Drill. Day Symposium.

[5]. Read, J. and Stacey, P. (2009). Guidelines for open pit slope design. CSIRO Publishing. 496 P.

[6]. Zare Naghadehi, M., Jimenez, R., KhaloKakaie, R. and Jalali, S.M.E. (2013). A new open-pit mine slope instability index defined using the improved rock engineering systems approach. Int. Journal of Rock Mechanics and Mining Sciences. 61: 1-14.

[7]. Ferentinou, M. and Fakir, M. (2018). Integrating Rock Engineering Systems device and Artificial Neural Networks to predict stability conditions in an open pit. Engineering Geology. 246: 293-309.

[8]. Santos, T.B., Lana. M.S., Pereira, T.M. and Canbulat, I. (2018). Quantitative hazard assessment system (Has-Q) for open pit mine slopes. Int Journal of Mining Science and Technology.

[9]. Clough, R.w. (1960). The Finite Element Method in Plane Stress Analysis. Proc, 2nd Conference of. Electronic and Computer of American Society of Civil Engineers.

[10]. Courant, R. (1943). Variational methods for the solution of problems of equilibrium and vibrations. Bulletin of American Mathematic Society. 49: 1-24.

[11]. Seed, H.B., Lee, K.L., Idriss, I.M. and Makdisi, R. (1973). Analysis of the Slides in the San Fernando Dams During the Earthquake of Feb 9. Earthquake Engineering Research Center. Report No. EERC 73-2. University of California. Berkeley.

[12]. Wilson, R.C. and Keefer, D. (1983). Dynamic analysis of a slope failure from the 6 August 1979 Coyote Lake, California, earthquake. Bulletin of Seismological Society of America. 73: 863-877.

[13]. Griffiths, D.V. and Prevost, J.H. (1988). Two- and Three-Dimensional Dynamic Finite Element Analyses of the Long Valley Dam. Geotechnique. 38: 367-388.

[14]. Prevost, J.H. (1981). DYNA-FLOW: a nonlinear transient finite element analysis program.

[15]. Elgamal, A.W.M., Scott, R.F., Succarieh, M.F. and Yan, L.J. (1990). La Villita Dam response during

five earthquakes including permanent deformation. Geotechnical. Engineering Division. ASCEV. 116. 1443-1462.

[16]. Latha, G.M. and Garaga, A. (2010). Seismic stability analysis of a himalayan rock slope. Rock Mechanics and Rock Engineering. 43: 831-843.

[17]. Jibson, R.W. (2011). Methods for Assessing the Stability of Slopes During Earthquakes, A retrospective. Engineering Geology. 122: 43-50.

[18]. Zhang, Y., Chen, G., Zen, K., Kasama, K. and Dong S. (2011). Limit Analysis of Seismic Slope Stability Based on Tension-Shear Failure Mechanism. 43: 18-28.

[19]. Morales-Esteban, A., De Justo, J.L., Reyes, J., Miguel Azañón, J., Durand, P. and Martínez-Álvarez, F. (2015). Stability analysis of a slope subject to real accelerograms by finite elements Application to San Pedro cliff at the Alhambra in Granada. Soil Dynamics and Earthquake Engineering. 69:28-45.

[20]. Jiang, X., Cui, P. and Liu, C. (2016). A chart-based seismic stability analysis method for rock slopes using Hoek-Brown failure criterion. Engineering Geology. 209: 196-208.

[21]. Azhari, A. and Ozbay, U. (2017). Investigating the effect of earthquakes on open pit mine slopes. Int. Journal of Rock Mechanics and Mining Sciences. 100: 218-228.

[22]. Kundu, J., Sarkar, K. and Singh, T.N. (2017). Static and Dynamic Analysis of Rock Slope- A Case Study. Proceeding of Engineering. 191: 744–749.

[23]. Lv, Q., Liu, Y. and Yang, Q. (2017). Stability analysis of earthquake-induced rock slope based on back analysis of shear strength parameters of rock mass. Engineering Geology. 228: 39-49.

[24]. Xiong, M. and Huang, Y. (2017). Stochastic seismic response and dynamic reliability analysis of slopes: A review. Soil Dynamics and Earthquake Engineering. 100: 458-464.

[25]. Fan, G., Zhang, L.M., Li, X.Y., Fan, R.L. and Zhang, J.J. (2018). Dynamic response of rock slopes to oblique incident SV waves. Engineering Geology. 247: 94-103.

[26]. Amini, M. and Ardestani, A. (2019). Stability analysis of the north-eastern slope of Daralou copper open pit mine against a secondary toppling failure. Engineering Geology. 249: 89-101.

[27]. Lin, C.H., Li, H.H. and Weng, M.C. (2018). Discrete element simulation of the dynamic response of a dip slope under shaking table tests. Engineering Geology. 243: 168-180.

[28]. Song, D., Che, A., Chen, Z. and Ge, X. (2018). Seismic stability of a rock slope with discontinuities under rapid water drawdown and earthquakes in large-scale shaking table tests. Engineering Geology. 245: 153-168.

[29]. Liu, Y.Q., Li, H.B., Zhao, J., Li, J.R. and Zhou, Q.C. (2004). Udec simulation for dynamic response of a rock slope subject to explosions. Int. Journal of Rock Mechanics and Mining Science. 41: 87198332.

[30]. Mohammadi Azizabadi, H.R., Mansouri, H. and Fouché, O. (2014). Coupling of two methods, waveform superposition and numerical, to model blast vibration effect on slope stability in jointed rock masses. Computers and Geotechnics. 61: 42-49.

[31]. Sangroya, R. and Choudhury, D. (2013). Stability Analysis of Soil Slope Subjected to Blast Induced Vibrations Using FLAC ^{3D}. Geo-Congress, Reston, VA: American Society of Civil Engineers. 472-881.

[32]. Jiang, N., Zhou, C., Lu, S. and Zhang, Z. (2017). Propagation and prediction of blasting vibration on slope in an open pit during underground mining. Tunnelling and Underground Space Technology. 70: 409-421.

[33]. Zheng, H., Li, T., Shen, J., Xu, C., Sun, H. and Lü, Q. (2018). The effects of blast damage zone thickness on rock slope stability. Engineering Geology. 246: 19-27.

[34]. Xiao, J., Gong, W., Martin, J.R., Shen, M. and Luo, Z. (2016). Probabilistic seismic stability analysis of slope at a given site in a specified exposure time. Engineering Geology. 212: 53-62.

[35]. Milne, G. and Davenport, A.G. (1969). Distribution of earthquake risk in Canada. Bulletin of Seismological Society of America. 59: 729-754.

[36]. McGuire, R.K. (2004). Seismic hazard and risk analysis. Oakland, Calif: Earthquake Engineering Research Institute.

[37]. Reiter, L. (1991). Earthquake hazard analysis: issues and insights. Columbia University Press.

[38]. Cornell, C. (1968). Engineering seismic risk analysis. Bulletin of Seismological Society of America. 58: 1583-1606.

[39]. Anderson, J.G. and Trifunac, M. (1978). Uniform risk functionals for characterization of strong earthquake ground motion. Bulletin of Seismological Society of America. 68: 205-218.

[40]. Zare, M., Bard, P.Y. and Ghafory Ashtiany, M. (1999). Site characterizations for the Iranian strong motion network. Soil Dynamics and Earthquake Engineering. 18: 101-123.

[41]. Mojarab, M., Memarian, H., Zare, M., Morshedy, A.M. and Pishahang, M.H. (2014). Modeling of the seismotectonic provinces of Iran using the self-organizing map algorithm. Computer and Geoscience. 67: 150-162.

[42]. BHRC n.d. (accessed July 26, 2018). http://smd.bhrc.ac.ir/Portal/en/BigQuakes/Details/27.

[43]. BHRC n.d. (accessed July 26, 2018) http://smd.bhrc.ac.ir/Portal/en/BigQuakes/Details/16.

[44]. BHRC n.d. (accessed July 26, 2018) http://smd.bhrc.ac.ir/Portal/en/BigQuakes/Details/40.

[45]. Berta, G. (1990). Explosives : an engineering tool. Italesplosivi.

[46]. Stead, D., Eberhardt, E. and Coggan, J.S. (2006). Developments in the characterization of complex rock slope deformation and failure using numerical modelling techniques. Engineering Geology. 83: 217-235.

[47]. Swan, C.C. and Seo, Y.K. (1999). Limit state analysis of earthen slopes using dual continuum/FEM approaches. Int. Journal of Numerical and Analytical Methods in Geomechanics. 23: 1359-1371.

[48]. Jing, L. and Hudson, J.A. (2002). CivilZone review paper - Numerical methods in rock mechanics. Int. Journal of Rock Mechanics and Mining Sciences. 39: 409-427.

[49]. Styles, T. (2009). Numerical Modelling and Analysis of slope stability within fracture dominated rock masses. PhD thesis. University of Exeter. 345 P.

[50]. Jing, L. (2003). A review of techniques, advances and outstanding issues in numerical modelling for rock mechanics and rock engineering. Int. Journal of Rock Mechanics and Mining Sciences. 40: 283-353.

[51]. Kani Kavan-e- Shargh Engineers. (2012). Seismic report and high separation rate monitoring network installation proposal. Chadormalu mine. 289 p. (in Persian).

[52]. Kuhlemeyer, R.L. and Lysmer, J. (1973). Finite element method accuracy for wave propagation problems. Journal of Soil Mechanics & Foundations Div, 99 (Tech Rpt).

[53]. Nakamura, Y. (1989). A method for dynamic characteristics estimation of subsurface using microtremor on the groundsurface. Quarterly Report of the Railwy Technical Research Institute. 30: 25-33.

[54]. Lysmer, J. and Kuhlemeyer, R.L. (1969). Finite Dynamic Model for Infinite Media. Journal of Engineering Mechanics Division. 95: 859-878.

[55]. Rayleigh, J.W.S. and Lindsay, R.B. (1945). The theory of sound. Dover.

[56]. Biggs, J.M. (1964). Introduction to structural dynamics. McGraw-Hill.

[57]. Landshoff, R. (1955). A Numerical Method for Treating Fluid Flow in the Presence of Shocks.

[58]. VonNeumann, J. and Richtmyer, R.D. (1950). A Method for the Numerical Calculation of Hydrodynamic Shocks. Journal of Applied Physics. 21: 232-237.

[59]. Sakuri, S., Hiraoka, A. and Hori, K. (1998). Strain induced damaged of rocks. Proc, 3rd Int. Conference of Mechanics of Jointed Faulted Rock, Wien. pp. 729-738.

[60]. Bishop, A.W. (1955). The use of the Slip Circle in the Stability Analysis of Slopes. Géotechnique. 5: 7-17.

مقایسه‌ای بین تأثیرهای زلزله و آتشباری بر پایداری شیروانی‌های معادن: مطالعه موردی معدن روباز چادرملو

روشنک شفیعی گنجه[1*]، حسین معماریان[1]، محمد حسین خسروی[1] و مسعود مجرب[2]

۱- دانشکده مهندسی معدن، دانشکده فنی، دانشگاه تهران، ایران

۲- شرکت مهندسین مشاور بنیان زمین پایدار، تهران، ایران

ارسال ۲۰۱۸/۱۰/۱۲، پذیرش ۲۰۱۹/۱/۱۶

* نویسنده مسئول مکاتبات: roshanakshafiei@ut.ac.ir

چکیده:

پایداری دینامیکی شیروانی‌ها در معادن روباز همچنان به عنوان یک مسئله چالش‌برانگیز در محاسبات طراحی معادن باقی‌مانده است. زلزله و آتشباری دو منبع حائز اهمیت از بارهای دینامیک هستند که می‌توانند در نواحی لرزه‌خیز و حین چرخه استخراج خسارت‌های بسیاری را به بار آورند. در این پژوهش، تأثیرهای زلزله و آتشباری بر پایداری شیروانی شمال غربی معدن چادرملو به وسیله یک روش مدل‌سازی عددی مقایسه شده است. نتایج دینامیک نشان می‌دهند که جابجایی حداکثر شیروانی تحت بارهای زلزله و آتشباری به ترتیب برابر با ۸۴۴ و ۱۴۶ میلی‌متر است. با توجه به نتایج کرنش برشی، هر دو موج زلزله و آتشباری مخرب هستند، درحالی‌که موج‌های زلزله خسارت بیشتری را به شیروانی وارد می‌کنند. علاوه بر این، تحلیل خطر لرزه‌ای تعیینی و احتمالاتی برای برآورد لرزه‌خیزی محدوده معدن انجام شده است. نتایج تجربی نشان می‌دهند که مقدار حداکثر شتاب قائم و افقی به ترتیب برابر با ۰/۵۵g و ۰/۷۵g است. سپس، شتاب حداکثر محاسبه شده به شتاب‌نگاشت‌های منتخب مقیاس شده است. به منظور نشان دادن تأثیر به سزای مقیاس انجام شده، مدل با استفاده از شتاب‌نگاشت‌های واقعی نیز اجرا شد. نتایج حاصل شده نشان دادند که مقیاس انجام شده از تخمین بیش از حد و کمتر از حد جابجایی و کرنش جلوگیری می‌کند؛ بنابراین، وارد کردن شتاب‌نگاشت‌های مقیاس شده در تحلیل پایداری دینامیکی شیروانی‌های معادن منجر به نتایج قابل اعتماد و استوارتری می‌شود. نتایج کلی نشان می‌دهد که یک زلزله قوی خسارت‌های زیادی به شیروانی وارد می‌کند و نتیجتاً منجر به توقف چرخه معدنکاری می‌شود؛ بنابراین، مطالعه لرزه‌ای و تحلیل پایداری دینامیک باید به عنوان بخشی از محاسبات طراحی معدن در نظر گرفته شود.

کلمات کلیدی: معدن چادرملو، تحلیل خطر لرزه‌ای، مدل‌سازی عددی، پایداری دینامیک شیروانی، زلزله، آتشباری.